Focused excimer laser initiated, radio frequency sustained high pressure air plasmas

Ryan Giar[a)] and John Scharer
Department of Electrical Engineering, University of Wisconsin-Madison, 506 Engineering Research Building, 1500 Engineering Drive, Madison, Wisconsin 53706, USA

(Received 5 August 2011; accepted 9 October 2011; published online 17 November 2011)

Measurements and analysis of air breakdown processes and plasma production by focusing 193 nm, 300 mJ, 15 MW high power laser radiation inside a 6 cm diameter helical radio frequency (RF) coil are presented. Quantum resonant multi-photon ionization (REMPI) and collisional cascade laser ionization processes are exploited that have been shown to produce high-density ($n_e \sim 7 \times 10^{16}/cm^3$) cylindrical seed plasmas at 760 Torr. Air breakdown in lower pressures (from 7–22 Torr), where REMPI is the dominant laser ionization process, is investigated using an UV 18 cm focal length lens, resulting in a laser flux of 5.5 GW/cm^2 at the focal spot. The focused laser power absorption and associated shock wave produce seed plasmas for sustainment by the RF (5 kW incident power, 1.5 s) pulse. Measurements of the helical RF antenna load impedance in the inductive and capacitive coupling regimes are obtained by measuring the loaded antenna reflection coefficient. A 105 GHz interferometer is used to measure the plasma electron density and collision frequency. Spectroscopic measurements of the plasma and comparison with the SPECAIR code are made to determine translational, rotational, and vibrational neutral temperatures and the associated neutral gas temperature. From this and the associated measurement of the gas pressure the electron temperature is obtained. Experiments show that the laser-formed seed plasma allows RF sustainment at higher initial air pressures (up to 22 Torr) than that obtained via RF-only initiation (<18 Torr) by means of a 0.3 J UV laser pulse. © *2011 American Institute of Physics*. [doi:10.1063/1.3660690]

I. INTRODUCTION

Air plasmas are of interest to a variety of industries such as defense, manufacturing, energy, and medicine. Specific applications include materials processing and certain kinds of device fabrication,[1] biological decontamination, environmental processing of noxious gases, medical sterilization,[2] and drag and radar cross-section reduction of aircraft.[3–6] Air plasmas have been produced and studied by various researchers for several decades and are still not well understood but historically have had high power budgets at higher pressures.[7–9] It is desired to rapidly produce large volume (100–1000 cm^3) air plasmas at high ($\sim$1000 Torr) pressures with minimum power requirements to reduce the cost and complexity of air plasma systems. Air plasmas are frequently and most commonly produced using inductively coupled antennas. Inductively coupled antennas operating at radio frequencies (RF) can be used for a multitude of applications, including plasma sources. With regard to the semiconductor industry, inductively coupled plasmas (ICP) are one of the most promising plasma sources because they have the advantages of independently controllable ion energy, reduction of ion damage to surrounding material, and high plasma density. Because of their ease of scalability, considerable research is presently focused on ICPs as the future of large area plasma sources. Outside of semiconductor wafer manufacturing, large area plasma sources can also be used for rapid bulk modification of other materials and substrates. One variant of the ICP reactor is the solenoidal type, having a helical coil wound around the side of the chamber. This coil can consist of hollow metal tubes cooled with water or oil (steady-state applications) or un-cooled solid metal straps or bars (pulsed applications); this experiment uses the former.

Previous work with inductively coupled air plasmas in our research group has involved a helical RF antenna and a low ionization energy seed gas.[10–15] This seed gas ($C_{10}N_4H_{16}$, tetrakis dimethylamino ethylene or TMAE) filled the plasma chamber to a low partial pressure (20 mTorr) compared to the flowing air (tens to hundreds of Torr) and was ionized by a large beam footprint (1 cm by 2.4 cm) excimer laser (argon fluoride, 193 nm). The laser photon energy is 6.42 eV and the ionization energy of TMAE is 6.1 eV. The initial background electron density provided by the ionized TMAE was measured to be on the order of $10^{13}/cm^3$. This enabled significant RF coupling early in the discharge, resulting in bulk ionization of the air and subsequent air plasma formation. These air plasmas extended significantly beyond the antenna region, occupying volumes on the order of hundreds of cm^3. They were determined to have steady state electron densities on the order of $10^{12}/cm^3$ and electron temperatures of 0.8 eV. The resulting RF power budget needed to sustain the inductive air plasma discharges was 5 W/cm^3. The major drawbacks to using TMAE as an initiator are the complicated and expensive synthesis process for

a)Author to whom correspondence should be addressed. Electronic mail: giar@wisc.edu.

TMAE, the toxic nature of this volatile organic compound, and the higher recombination rates that reduce the plasma lifetime compared to air only (no TMAE) cases. An alternative initiation mechanism that is safer but also noninvasive is highly sought for the production of large volume, high density air plasmas. To that end, we employ our excimer laser in a unique fashion to seed air without the use of other gases. We also examine the properties of capacitive and inductive coupling of RF power to air plasmas.

II. THEORETICAL BACKGROUND

A. Laser focus breakdown

Through the use of a high transmissivity focusing compound microscope system or single parabolic lens the laser beam can be concentrated to very high fluxes (10^9 to 10^{12} W/cm^2).[16,17] The very high photon population causes ionization in air through intense electric fields via collisional cascade (classical effect) and resonance multi-photon ionization (quantum process). The ionization energies of nitrogen and oxygen are 15.6 eV and 12.1 eV, respectively. As such, only two or three photons from our laser are required to ionize any of the major constituents of air provided these photons are absorbed on a time scale faster than the excited state deexcitation time. To that end, there exists a resonance enhanced multi-photon ionization (REMPI) process for air. This process involves at least one photon that is absorbed by an air molecule that creates a relatively long-lived metastable state. This resonance excited molecule can then absorb another photon, resulting in ionization. Because nitrogen has an ionization energy approximately 2.5 times the laser photon energy, this $2+1$ REMPI process contributes significantly to the ionization of neutral air and to the electron density of the air plasma. Additionally, oxygen has an ionization energy slightly less than two times the laser photon energy. There is a $1+1$ REMPI process for oxygen and its excited metastable state can couple to the nitrogen via collisions. Recent work by Hummelt *et al.* has shown, by mixing oxygen and nitrogen concentrations, that oxygen REMPI processes play a critical role in 193 nm laser breakdown of air.[17] These quantum effects significantly lower the power fluxes needed for air breakdown compared with classical processes by a factor of 1000 for our laser in air.[16,18] Previous studies of these laser focus plasmas with an 18 cm focal length lens producing 5.5 GW/cm^2 fluxes at atmospheric pressure have revealed very high electron densities ($\sim 10^{16}$/cm^3), far in excess of the densities of the laser TMAE plasmas ($\sim 10^{13}$/cm^3) albeit at much smaller volumes.[16] Nevertheless, it is believed that these high density, small volume laser sparks can contribute significantly to high pressure breakdown initiation and can assist in producing large volume, RF sustained air plasmas.

B. RF sustainment

After plasma initiation by the 18 cm focused laser, the small plasmoid ($\sim$mm by $\sim$cm) located in the antenna region is energized with RF through a 5-turn helical antenna. This causes the plasmoid to grow through further ionization of the surrounding neutral gas. The plasma dynamics are largely characterized by the neutrals and the electrons. The neutrals are heated by the electrons and the ions are cooler due to their lower concentration and low energy exchange cross section with the electrons. However, the electrons in our RF-heated air plasmas will have significantly higher temperatures than the neutrals. This is due to the greater number of processes by which neutrals can lose energy compared with electrons. Whereas electrons can only lose energy by colliding with neutrals and ions, the neutrals can lose energy through convection and radiative emission by collisions with electrons and other neutrals.[12–15] Additionally, there are two modes through which our antenna couples to the air plasmas at these incident 5 kW power levels. The lower pressure mode is the inductive mode (H-mode), characterized by higher electron density and higher plasma resistance. The higher pressure mode is the capacitive mode (E-mode), characterized by lower electron density and lower plasma resistance. Additionally, the H-mode is much more luminous than the E-mode. This can be seen from our RF plasma photos shown in Figs. 1 and 2. For purposes of this research, our RF power is set to a constant value of 5 kW to limit the power budget needed for RF sustainment of our plasmas, which requires optimization of the antenna and matching network.

C. Plasma impedance diagnostic

The RF power is coupled to the antenna-plasma system via a capacitive impedance matching network. The particular circuit employed is referred to as the alternate circuit.[12] A schematic of the circuit is shown in Fig. 3. Through use of a dual directional coupler the complex reflection coefficient (magnitude and phase) is measured to determine the efficiency of the matching network. The typical operational routine involves dialing the capacitors to known values and firing a plasma shot, then measuring the reflection coefficient. With that information the plasma-loaded antenna impedance Z_L can be determined from the following equations,

$$Z_{in} = Z_1 + \left(\frac{1}{Z_2} + \frac{1}{Z_L}\right)^{-1} = Z_0\left(\frac{1+\Gamma_{in}}{1-\Gamma_{in}}\right) \ [\Omega], \tag{1}$$

$$Z_L = Z_2\left(\frac{Z_{in} - Z_1}{Z_1 + Z_2 - Z_{in}}\right) \ [\Omega]. \tag{2}$$

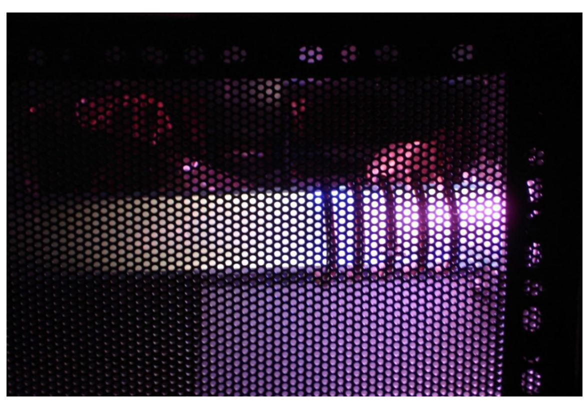

FIG. 1. (Color online) Photo of typical E-mode air plasma (5 kW forward RF power at 20 Torr).

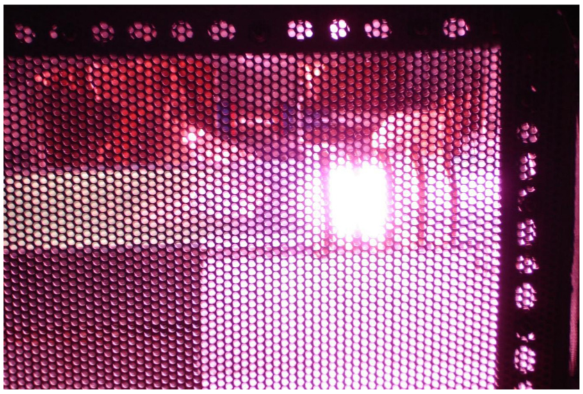

FIG. 2. (Color online) Photo of typical H-mode air plasma (5 kW forward RF power at 10 Torr).

Here Γ_{in} is the input reflection coefficient and Z_{in} is the input impedance, with *in* denoting the input to the matchbox (before the matching circuit). Also, Z_0 is the transmission line impedance (50 Ω) and Z_1 and Z_2 are the impedances of the capacitors. Once the steady-state plasma impedance is known then the matched capacitances can be calculated by using ideal circuit equations derived for the alternate circuit, which assume no reflections ($\Gamma_{in}=0$). The matched settings for the capacitors are given by:

$$C_1 = \frac{R_L}{\omega_{RF} g_L Z_0} \ [\mathrm{F}], \tag{3}$$

$$C_2 = \frac{X_L - g_L}{(X_L^2 + R_L^2)\omega_{RF}} \ [\mathrm{F}], \tag{4}$$

$$g_L = \left(\frac{R_L}{Z_0}\right)^{\frac{1}{2}} \left(X_L^2 + (R_L - Z_0)R_L\right)^{\frac{1}{2}} \ [\Omega]. \tag{5}$$

Here R_L is the load resistance and X_L is the load reactance with ω_{RF} being the frequency of the RF generator (13.56 MHz). The vacuum load (no plasma) antenna impedance Z_A is measured by means of a network analyzer to be 0.5 + j150 Ω. Due to the helical antenna, the plasma coupling impedance will be in parallel with the vacuum antenna impedance.[19] The capacitors are adjusted until the reflection coefficient is minimized. This is done to maximize RF power coupling into the plasma that in turn minimizes the overall plasma power budget. Note that E-mode and H-mode plasmas have significantly different impedances, which complicates the impedance matching process. Because it is desirable to produce H-mode discharges due to the higher electron density, the matching procedure is focused mainly on the H-mode resistance and reactance. It is also easier to produce H-mode plasmas at lower pressures, but at higher pressures only E-mode discharges were produced at the fixed capacitor settings so it is necessary to characterize the E-mode impedance as well.

D. Millimeter wave interferometry

The plasma electron density n_e and electron-neutral collision frequency υ are measured using a millimeter wave interferometer. The millimeter wave beam is phase shifted and attenuated by its interaction with the collisional air plasma. From this interaction the attenuation and phase constants α_p and β_p of the plasma are determined. These quantities are given by:[13,15]

$$\alpha_p = \left(\frac{\omega^2}{2c^2}\right)^{\frac{1}{2}} \left(\frac{\omega_p^2}{\omega^2+\upsilon^2} - 1 + \left(\frac{\omega_p^4 - 2\omega^2\omega_p^2 + \omega^2\upsilon^2 + \omega^4}{\omega^4 + \upsilon^2\omega^2}\right)^{\frac{1}{2}}\right)^{\frac{1}{2}} \ [\mathrm{Np/m}], \tag{6}$$

$$\beta_p = \left(\frac{\omega^2}{2c^2}\right)^{\frac{1}{2}} \left(1 - \frac{\omega_p^2}{\omega^2+\upsilon^2} + \left(\frac{\omega_p^4 - 2\omega^2\omega_p^2 + \omega^2\upsilon^2 + \omega^4}{\omega^4 + \upsilon^2\omega^2}\right)^{\frac{1}{2}}\right)^{\frac{1}{2}} \ [\mathrm{rad/m}]. \tag{7}$$

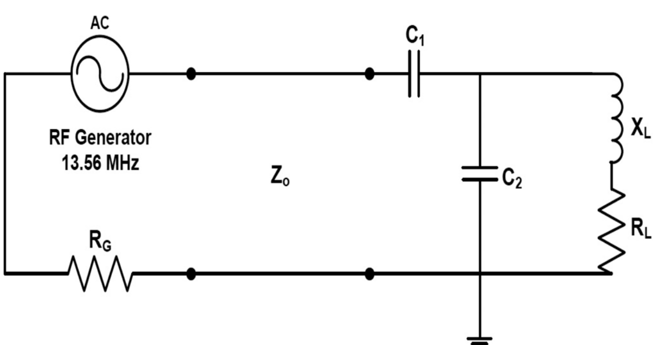

FIG. 3. Circuit diagram of impedance matching network.

Here c is the speed of light and ω is the interferometer frequency. In this experiment these line averaged quantities are measured according to these approximations:

$$\Delta\phi \approx \left(\beta_0 - \beta_p\right)D \ [\mathrm{rad}], \tag{8}$$

$$A \approx A_0 \exp\left(-\alpha_p D\right) \ [\mathrm{Np}]. \tag{9}$$

Here the measured phase shift is $\Delta\phi$ and the measured attenuation is A/A_0 with the plasma diameter given by D where we are assuming line average values. By inverting Eq. (6) and Eq. (7) the plasma and collision frequencies can be derived:[13–15]

$$\upsilon = \frac{2\omega\alpha_p\beta_p c^2}{(\alpha_p-\beta_p)(\alpha_p+\beta_p)c^2+\omega^2}\ [\text{rad/s}], \tag{10}$$

$$\omega_p = \left(c^2(\alpha_p-\beta_p)(\alpha_p+\beta_p)+\omega^2 + \frac{4c^4\alpha_p^2\beta_p^2}{\omega^2+(\alpha_p+\beta_p)(\alpha_p-\beta_p)c^2}\right)^{\frac{1}{2}}\ [\text{rad/s}]. \tag{11}$$

The electron density is easily determined from the plasma frequency. It should be noted that the interferometer diagnostic is line-of-sight and the collision frequency and electron density are line-averaged along the diameter. The electron temperature T_e can be obtained indirectly by expressing the collision frequency in terms of a temperature-dependent cross section $\sigma(T_e)$:[13,15]

$$\upsilon = n_n\sigma(T_e)v_e\ [\text{Hz}], \tag{12}$$

$$k_BT_e = \frac{m_e\pi}{8}\left(\frac{\upsilon}{n_n\sigma(T_e)}\right)^2\ [\text{J}]. \tag{13}$$

Here m_e is the electron mass, v_e is the electron velocity (rewritten in terms of temperature assuming a three-dimensional Maxwellian distribution of velocities), and n_n is the neutral density. Once the collision frequency and neutral density are known then the electron temperature can be determined by iteratively solving Eq. (13) using a polynomial fit for the collision (electrons on neutrals) cross section. The neutral density is determined by measuring the gas pressure during the RF heating with a gauge and later measuring the neutral temperature via spectroscopic means.

E. Optical emission spectroscopy

The temperature of the neutral air background gas T_g is measured by means of a spectrometer. The emission spectra of the plasma are examined and several prominent lines are isolated. These experimentally measured emission lines are compared to the theoretical emission spectra as calculated by a program called SPECAIR.[8] Because the plasmas are highly collisional, the various temperatures associated with the degrees of freedom of molecules (translational, vibrational, rotational) are expected to be comparable to one another. These temperatures in SPECAIR are manually adjusted in increments of 100 K until the theoretically calculated spectra graphically match the experimentally measured emission spectrum from the air plasmas. An example of this is shown in Fig. 4 for the 336.8 nm nitrogen line. The experimentally measured spectrum is in red and the SPECAIR calculated spectrum is in blue. Because the pressure of the neutral gas is known from a pressure gauge, the neutral density is known once the neutral temperature is established.

III. EXPERIMENTAL SETUP

The experiment consists of a 2 in. diameter, 40 in. long Pyrex® tube that serves as the plasma chamber. A 5-turn, water cooled, copper tube helical antenna is wound around

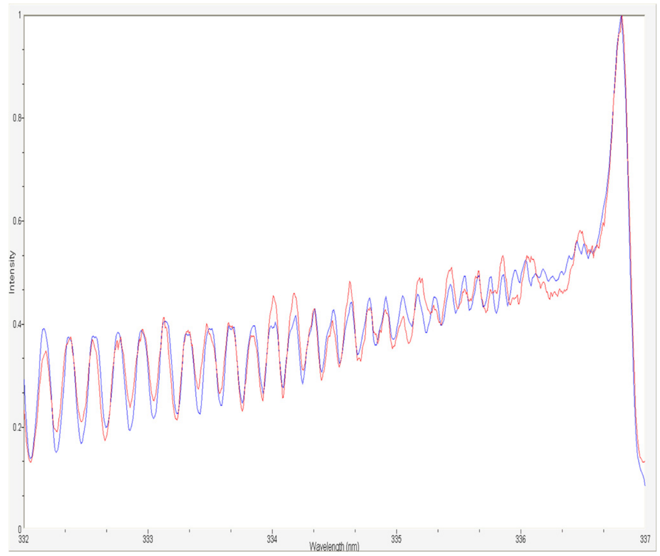

FIG. 4. (Color online) Typical 3500 K SPECAIR fit for the 336.8 nm line in air.

the Pyrex® tube. It has a diameter of 3 in. and a length of 4.5 in with 0.75 in. spacing between the turns. The antenna has a measured vacuum impedance of $0.5 + j150\ \Omega$. The RF generator is a 25 kW, 13.56 MHz vacuum tube based device that transfers power via a 50 Ω coaxial transmission line. This cable is connected to the dual directional coupler, which itself is connected to the impedance matchbox. The matchbox consists of one grounded vacuum variable capacitor that is in parallel with the antenna and one floating capacitor that is in series with the grounded capacitor and antenna. As mentioned earlier, the directional coupler is used to determine the reflection coefficient by measuring the incident and reflected voltages from the plasma loaded antenna. Shielding is provided by a perforated aluminum cage constructed around the Pyrex® tube and connected to the impedance matchbox. Figure 5 shows a diagram of the lab setup.

The excimer laser operates in the argon-fluoride mode that produces 193 nm radiation (6.42 eV per photon). The energy output is 300 mJ over 20 ns that translates to 15 MW. This is focused to a small spot size with a calcium-fluoride convex lens with a focal length of 18 cm. The spot is formed inside the center of the Pyrex® chamber near the front of the helical antenna.

The interferometer is arranged in a Mach-Zender configuration with the millimeter wave beam passing through the diameter of the plasma, centered just 3 cm past the front (hot-lead) of the antenna. The millimeter wave source is a Gunn oscillator operating at a frequency of 105 GHz and transmitted through W-band waveguides and a standard gain horn antenna (an identical horn serves as the receiver). The millimeter wave beam-width is 20° (due to the tapering angle of the horn antennas) and the signal is mixed with itself after a 90° phase shift and then further mixed with the portion of the signal that traverses the plasma. This mixing occurs in special mixer diodes that produce two signals: in-phase and quadrature-phase. These signals are treated as x-y coordinates in Cartesian space with the change in angle representing the phase shift and the change in radius

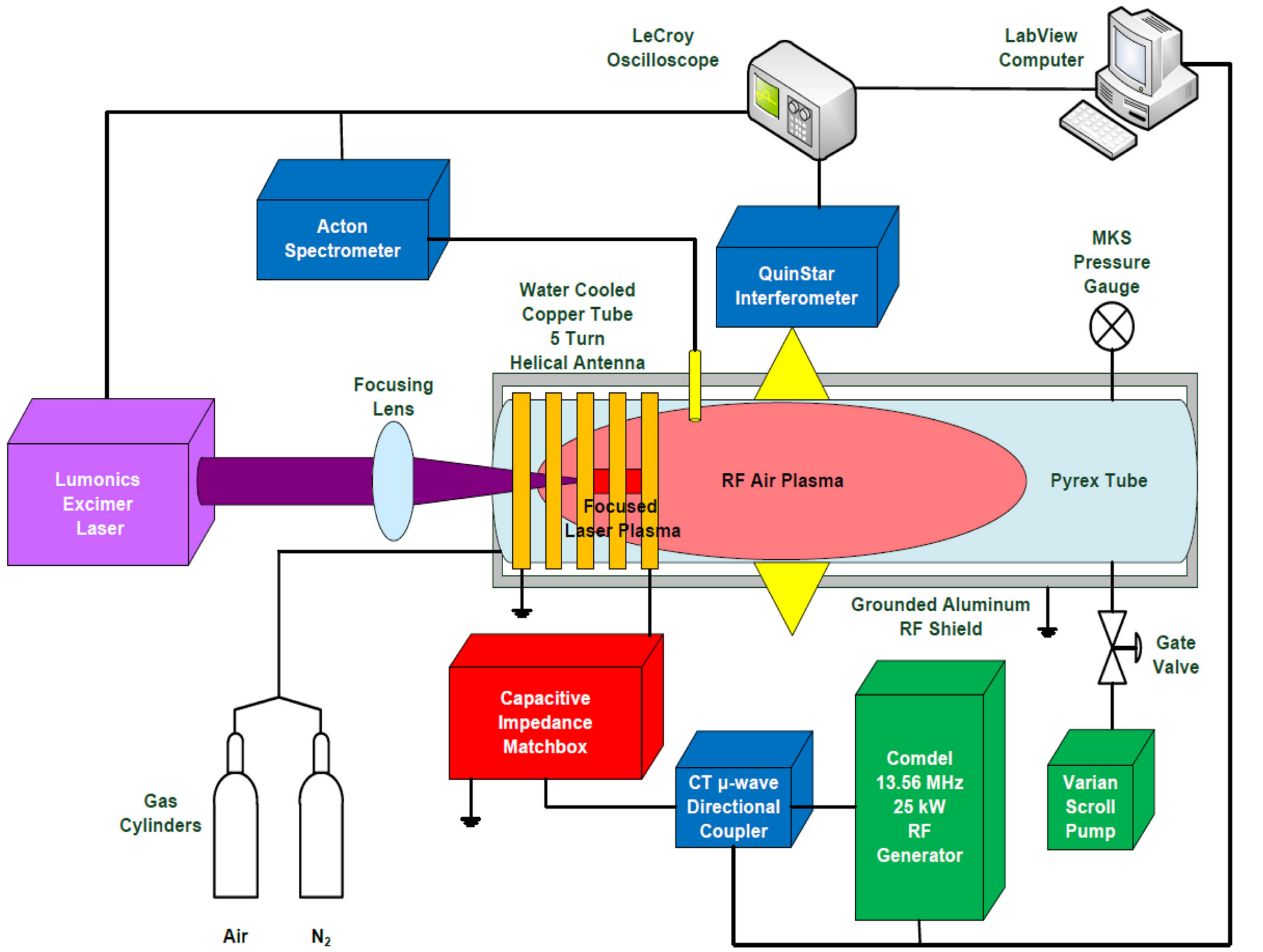

FIG. 5. (Color online) Illustration of the laser initiated, RF sustained air plasma experiment.

representing the attenuation. The raw interferometer traces are shown graphically for E- and H-modes in Fig. 6. The vacuum calibration circle is in blue and the plasma trace is in red.

The spectrometer captures light emitted from the plasma by means of a collimating lens and fiber optic cable. The main nitrogen lines of interest are 336.8 nm, 391.2 nm, and 427.5 nm. The measured spectra are imported into the SPECAIR code and then the various temperatures are set and adjusted until the calculated spectrum matches the measured spectrum. The best-fit temperature average is the neutral temperature of the background air gas.[8]

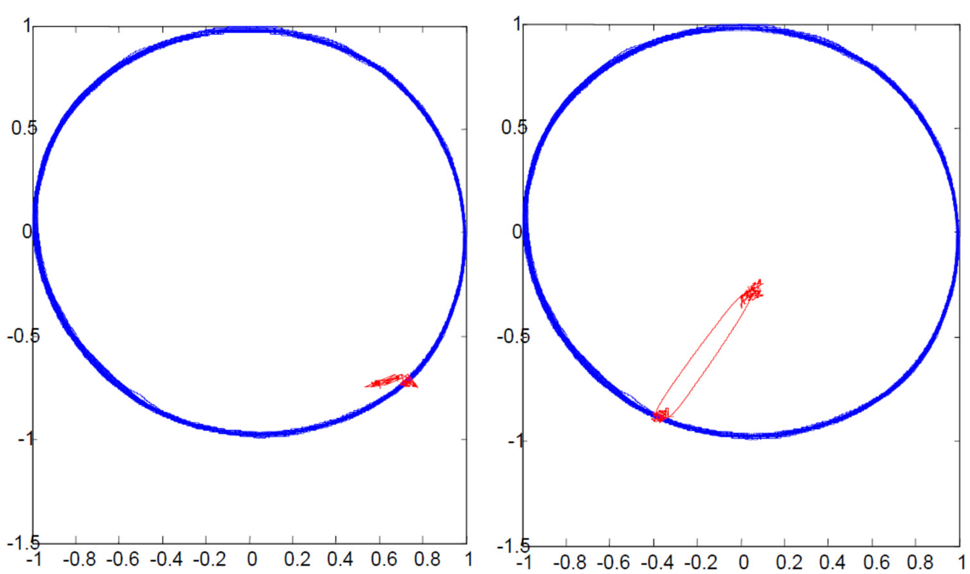

FIG. 6. (Color online) Characteristic in-phase/quadrature-phase millimeter wave interferometer traces for E-mode (left) and H-mode (right), with the circle representing the vacuum calibration and the elongated smudge signaling the plasma shot.

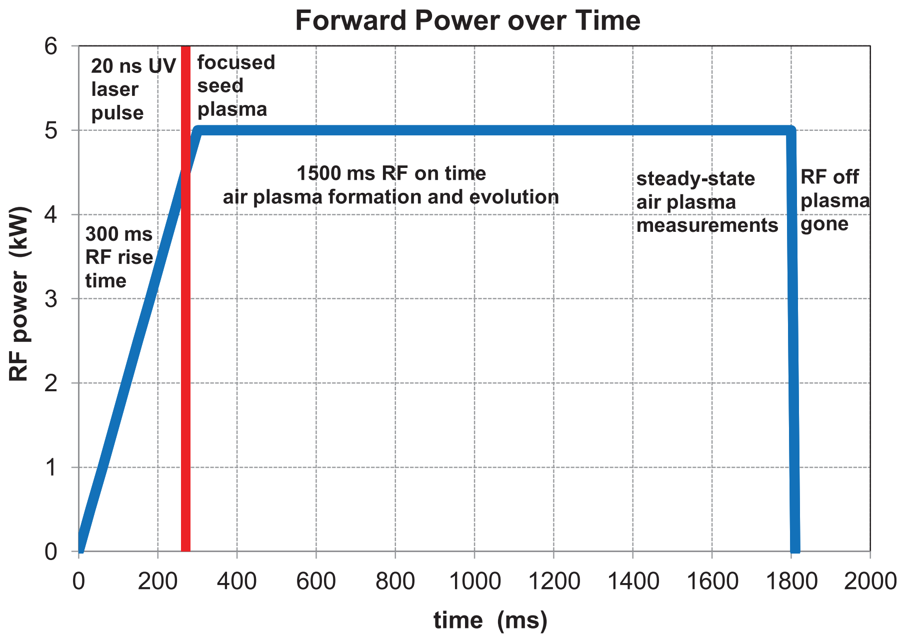

FIG. 7. (Color online) Plot of the timings of the RF generator and UV laser.

IV. RESULTS AND ANALYSIS

Pressure scans were conducted using just the RF to determine what maximum start-up pressure was attainable with just 5 kW of incident RF power. The RF on time is 1500 ms, with steady state plasma measurements being done between 1300 ms and 1400 ms. Later the laser focus seed plasma was incorporated into the experiment to increase the start-up pressure even further. H-mode discharges at this power level (5 kW) were possible up to 12 Torr. Beyond this only E-mode discharges were possible, up to 18 Torr. Ten shots at each pressure were carried out to determine these limits. Beyond this pressure it was no longer possible to form an air plasma at all at this 5 kW forward power level. At this point the laser focus initiation mechanism was utilized. The laser was timed to fire 295 ms after the RF enable signal was triggered (the RF has a rise time of 300 ms). The timings are shown graphically in Fig. 7. The laser is fired twice with a rep rate of 10 Hz; this is done because occasionally there is a misfire with the laser and the excimer reaction does not occur. With laser focus seeding the RF was able to sustain large volume discharges up to 22 Torr, all of which were E-mode. The following plots in Figs. 8–12 are pressure scans of various plasma quantities with 5 kW of incident RF power.

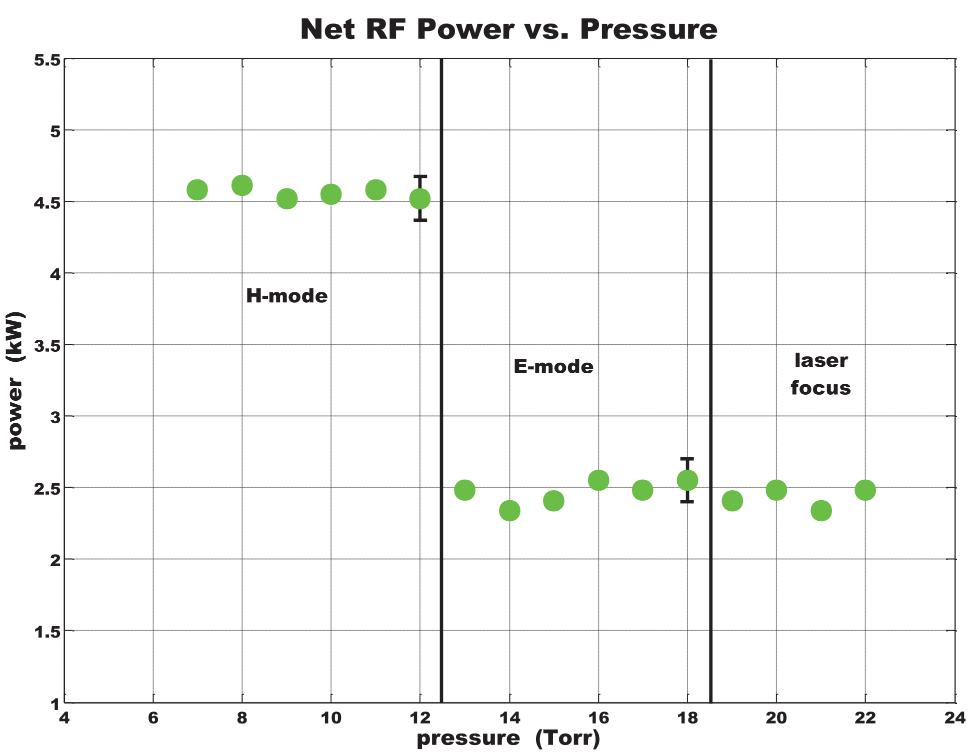

FIG. 8. (Color online) Pressure scan of net coupled RF power.

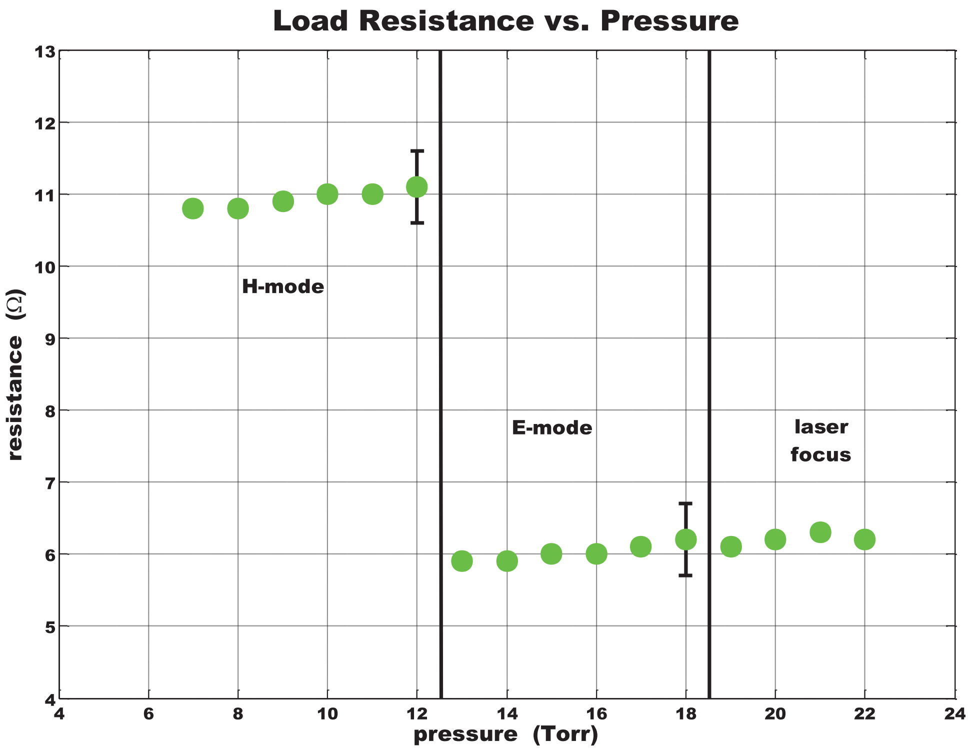

FIG. 9. (Color online) Pressure scan of plasma-loaded antenna resistance.

The H-mode discharges have an average voltage reflection coefficient magnitude (Γ) of 0.3 while the E-mode discharges have an average Γ of 0.7. This corresponds to power reflection coefficients of 9% and 49%, respectively, so that the average net power coupled to the plasma is 4.6 kW for the H-mode cases and 2.5 kW for the E-mode cases. This is due to the increased difficulty of matching to a capacitive load with an inherently inductive element (helical antenna) and creating plasma with the initial vacuum loaded antenna while also sustaining the higher density steady state conditions with fixed capacitor settings, all on ms time scales. As a result the net power coupled to the H-mode case is approximately 2 kW higher than for the E-mode case, as seen in Fig. 8.

As shown in Fig. 9 the average H-mode total plasma-antenna resistance is 11 Ω while the average E-mode total plasma-antenna resistance is 6 Ω, as determined from reflection coefficient measurements. This decrease in resistance is exactly what is expected because the resistance depends on the electron density which decreases sharply when

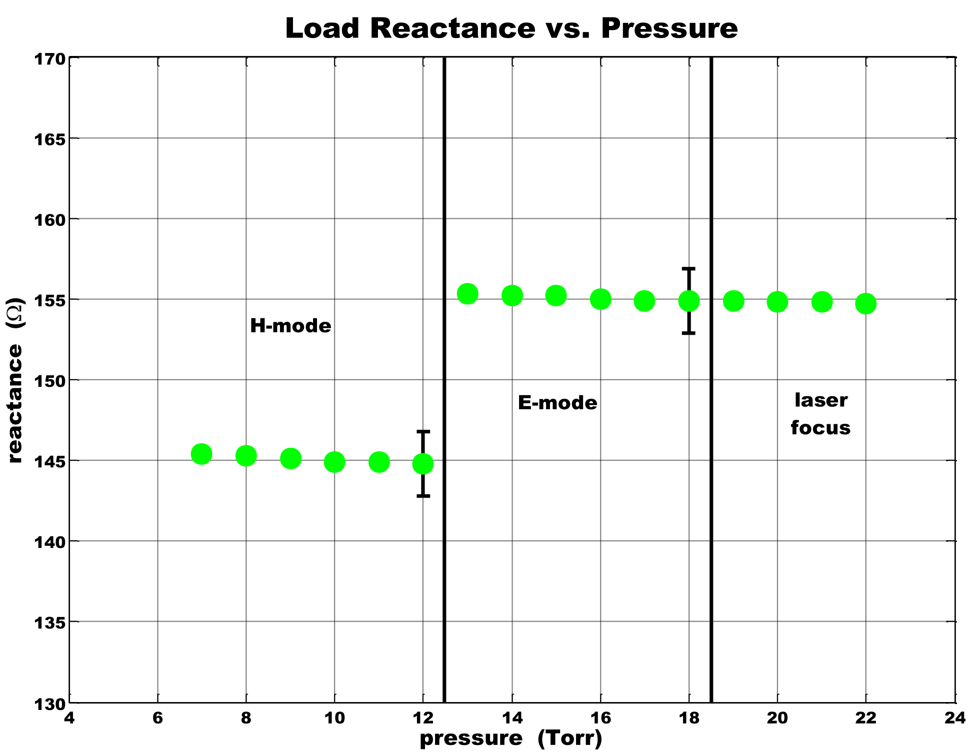

FIG. 10. (Color online) Pressure scan of plasma-loaded antenna reactance.

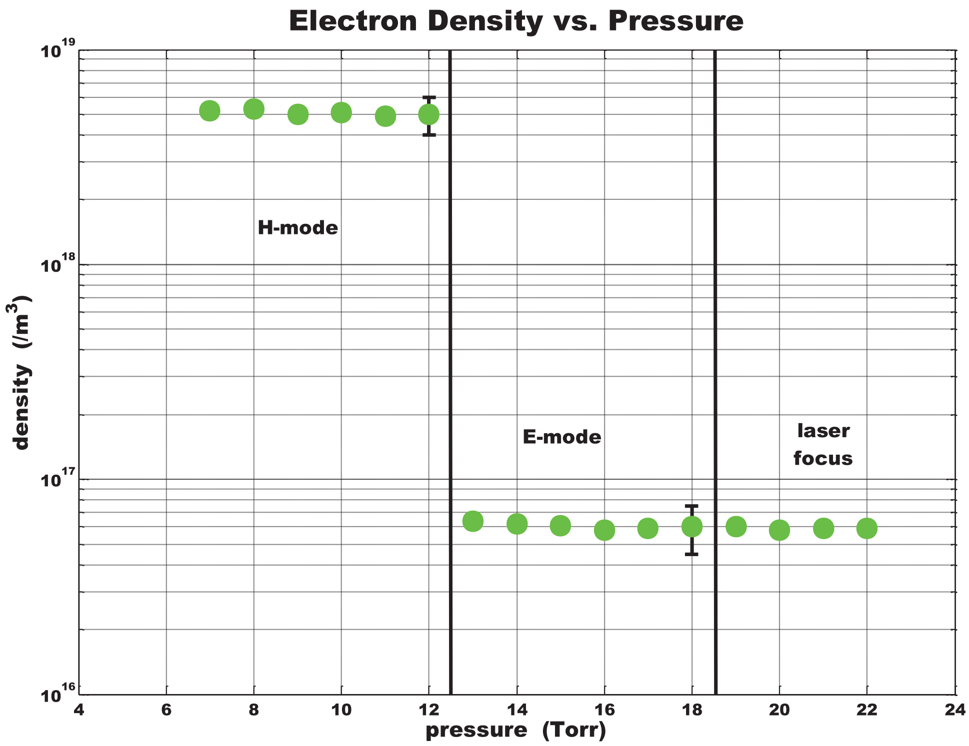

FIG. 11. (Color online) Pressure scan of electron density.

transitioning from inductive to capacitive coupling. For the same reason the plasma-loaded antenna reactance increases (see Fig. 10), with H-mode having an average load reactance of 145 Ω and E-mode having an average load reactance of 155 Ω. The changes in impedance correspond to the plasma antenna loading occurring in parallel with the helical coil.[19]

There is a two-order-of-magnitude decrease in the electron density going from the H-mode at low pressures to the E-mode at high pressures, as seen in Fig. 11. The H-mode has an average electron density of $\sim 5 \times 10^{12}/\mathrm{cm}^3$ while the E-mode has an average electron density of $6 \times 10^{10}/\mathrm{cm}^3$. Note that these densities are lower bounds for the plasma that is brighter under the helical coil. This is the main characteristic differentiating inductive from capacitive coupling. The collision frequency changes monotonically with pressure and does not have a sharp mode dependence because these air plasmas are neutral dominated. The average collision frequency over the pressure range (7 Torr to 22 Torr) increases from 6–9×10^{10} Hz.

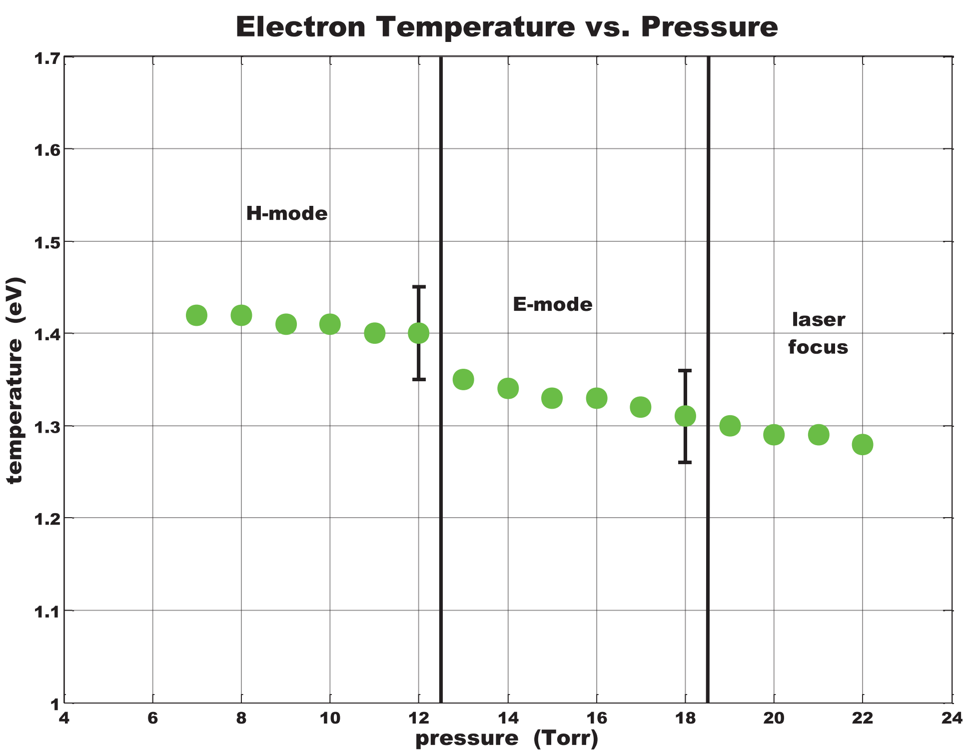

FIG. 12. (Color online) Pressure scan of electron temperature.

The neutral temperature is measured to be 3500 K for all pressures (including laser focus) and for both modes. From this the neutral density variation with pressure can be determined. Neutral density is then combined with the collision frequency via Eq. (13) to calculate the electron temperature variation with pressure (see Fig. 12). This results in an electron temperature of 1.4 eV for the H-mode and 1.3 eV for the E-mode. A slightly cooler T_e is expected for E-mode because the neutral population is considerably higher than that of H-mode. These values at lower pressures (10–20 Torr) show a slightly higher electron density and significantly higher electron temperature than the TMAE produced plasmas created by Luo *et al*. at comparable power levels and higher pressures in TMAE.[14,15] Although the laser produced plasmas can be created at higher initial pressures, the final E-mode steady state plasma conditions are comparable to the RF only cases because the laser energy is $< 0.1\%$ of the total energy coupled to the plasma.

V. CONCLUSIONS AND SUMMARY

We have demonstrated that it is possible to increase the RF-sustained start-up pressure of air plasmas with the aid of UV laser focus formed plasma seeds. A 4 Torr increase over RF only start-up pressures represents a 22% pressure range improvement in RF air plasma formation with only a 0.1% energy increased contribution from the laser pulse. The sustainment of the laser formed plasma above 20 Torr also validates that REMPI processes in air at these pressures (as seen in earlier UV laser works)[16,17] do occur and dominate the seed ionization process in this range at laser power fluxes well below (10^{-3}) the classical collisional cascade threshold flux of 1 $\mathrm{TW/cm^2}$. Our plasma volumes are nearly double our antenna volume at 300 $\mathrm{cm^3}$. This translates to a modest power budget of 15 $\mathrm{W/cm^3}$. Additionally we have demonstrated that large volume, moderate density ($5 \times 10^{10}/\mathrm{cm^3}$) plasmas at moderate power levels (2.5 kW) can be created in high pressure air with the aid of the laser focus seed plasma ionization. Electron temperatures of 1.3 eV were measured for both E-mode RF-only and laser-initiated air plasmas. With a neutral gas temperature of 3500 K, clearly our plasmas are not in local thermodynamic equilibrium (non-LTE) because the electrons are much hotter. The main reasons for this are radiative losses via meta-stable excitations in the neutral air molecules.

ACKNOWLEDGMENTS

This research was supported by the Air Force Office of Scientific Research Grant FA9550-09-1-0357.

[1] P. Tsai, L. Wadsworth, and J. R. Roth, Textile Res. J. **67**, 359 (1997).
[2] K. Kelly-Wintenberg, T. C. Montie, C. Brickman, J. R. Roth, A. K. Carr, K. Sorge, L. C. Wadsworth, and P. P. Y. Tsai, J. Ind. Microbiol. Biotechnol. **20**(1), 69 (1998).
[3] K. L. Kelly, J. E. Scharer, G. Ding, M. Bettenhausen, and S. P. Kuo, J. Appl. Phys. **85**(1), 63 (1999).
[4] R. J. Vidmar, IEEE Trans. Plasma Sci. **18**, 733 (1990).
[5] R. J. Roth, 44th Annual Meeting of the Division of Plasmas, American Physical Society, abstract #CI2.006 (2002).
[6] M. Laroussi, Int. J. Infrared Millim. Waves **17**, 2215 (1996).
[7] R. J. Vidmar and K. R. Stalder, Proceedings of the AIAA, 2003, pp. 1–8.
[8] C. O. Laux, T. G. Spencer, C. H. Kruger, and R. N. Zare, Plasma Sources Sci. Technol. **12**, 125 (2003).
[9] K. R. Stalder, R. J. Vidmar, G. Nersisyan, and W. G. Graham, J. Appl. Phys. **99**(9), 093301 (2006).
[10] K. Akhtar, J. E. Scharer, S. Tysk, and C. M. Denning, IEEE Trans. Plasma Sci. **32**, 813 (2004).
[11] G. Ding, J. E. Scharer, and K. Kelly, Phys. Plasmas **8**(1), 334 (2001).
[12] K. L. Kelly, J. E. Scharer, E. S. Paller, and G. Ding, J. Appl. Phys. **92**(2), 698 (2002).
[13] S. Luo, "Atmospheric pressure laser initiated and radiofrequency sustained plasmas," Ph.D. thesis (University of Wisconsin–Madison, 2007).
[14] S. Luo, J. E. Scharer, M. Thiyagarajan, and C. M. Denning, IEEE Trans. Plasma Sci. **34**(6), 2637 (2006).
[15] S. Luo, C. M. Denning, and J. E. Scharer, J. Appl. Phys. **104**, 013301 (2008).
[16] J. Way, J. Hummelt, and J. Scharer, J. Appl. Phys. **106**, 083303 (2009).
[17] J. Hummelt and J. Scharer, J. Appl. Phys. **108**, 093305 (2010).
[18] G. Bekefi, *Principles of Laser Plasmas* (Wiley, New York, 1976), pp. 457–508.
[19] M. A. Lieberman and A. J. Lichtenberg, *Principles of Plasma Discharges and Materials Processing*, 2nd ed. (Wiley, New York, 2005).